Spin-Orbit Torques in Heavy-Metal–Ferromagnet Bilayers with Varying Strengths of Interfacial Spin-Orbit Coupling

Lijun Zhu, D. C. Ralph, and R. A. Buhrman

Phys. Rev. Lett. **122**, 077201 — Published 19 February 2019

DOI: 10.1103/PhysRevLett.122.077201

Spin-orbit torques in heavy metal/ferromagnet bilayers with varying strength of interfacial spin-orbit coupling

Lijun Zhu,[1]* D. C. Ralph,[1,2] and R. A. Buhrman[1]
1. Cornell University, Ithaca, NY 14850
2. Kavli Institute at Cornell, Ithaca, New York 14853, USA
*e-mail: lz442@cornell.edu

Despite intense efforts it has remained unresolved whether and how interfacial spin-orbit coupling (ISOC) affects spin transport across heavy metal (HM) / ferromagnet (FM) interfaces. Here we report conclusive experiment evidence that the ISOC at HM/FM interfaces is the dominant mechanism for "spin memory loss". An increase in ISOC significantly reduces, in a linear manner, the dampinglike spin-orbit torque (SOT) exerted on the FM layer via degradation of the spin transparency of the interface for spin currents generated in the HM. In addition, the fieldlike SOT is also dominated by the spin Hall contribution of the HM and decreases with increasing ISOC. This work reveals that ISOC at HM/FM interfaces should be *minimized* to advance efficient SOT devices through atomic layer passivation of the HM/FM interface or other means.

Key words: spin orbit torque, spin Hall effect, spin orbit coupling, spin transparency

Current-induced spin-orbit torques (SOTs) in heavy metal/ferromagnet (HM/FM) systems have attracted remarkable attention due to their potential for the efficient manipulation of magnetization in metals and insulators at the nanoscale [1-5]. When the spin Hall effect (SHE) of the HMs is the dominant source of the SOTs as is the case for many HM/FM systems [4,6], achieving high spin transparency (T_{int}) at the HM/FM interfaces is of the same importance as achieving a large spin Hall ratio (θ_{SH}) in the HMs for obtaining a large dampinglike SOT efficiency per *unit bias current density* $\xi^j_{DL} \equiv T_{int}\theta_{SH}$, the quantity of primary importance for efficiently driving magnetization switching [1,2,4,6], magnetization dynamics, and chiral spin texture displacement [3]. Recently, it has become recognized that so-called "spin memory loss" (SML) at many HM/FM interfaces can degrade T_{int} [7-9] and therefore substantially reduce the spin current that is pumped into the HM by a resonantly excited FM, or alternatively reduce the ξ^j_{DL} exerted on the FM layer by spin current arising from the SHE in the HM. While intermixing and atomic disorder were initially expected to be the dominant cause of SML, an extended first-principles analysis of spin pumping by Zwierzycki *et al*. [10] indicates that the spin mixing conductance $G^{\uparrow\downarrow}$ of a HM/FM interface is insensitive to interfacial diffusion and atomic disorder. Thus a different explanation for SML is required.

The initial spin-pumping theories and the supporting experiments omitted any effects of the interfacial spin-orbit coupling (ISOC) at the HM/FM interface and assumed the (pumped) spin current to be continuous across the HM/FM interface [7,11-13]. More recently, a number of theoretical efforts [14,15] have been made to assess the possible relevance of ISOC to T_{int} and the SOT efficiencies. Some calculations have suggested that ISOC at the HM/FM interface could contribute to SML [16,17], acting to enhance the spin scattering at the interface even in absence of inter-diffusion or atomic disorder [18]. However, clear experimental evidence for whether and how ISOC is relevant in SOTs and T_{int} has been lacking, as it is a major challenge to engineer and quantify a changing strength of ISOC within one material system while keeping the SOT efficiencies high enough to measure accurately.

In this letter, we demonstrate that ISOC at Pt/Co and $Au_{0.25}Pt_{0.75}$/Co interfaces can be tuned significantly via thermal engineering of the spin-orbit proximity effect. From this ability we show that ISOC is the dominant mechanism for SML and reduces the dampinglike SOT efficiency by degrading T_{int} in a linear manner. We also find that the fieldlike torque is dominated by the SHE of the HM and is affected by ISOC only via degradation of T_{int}. The ISOC-generated SOTs is found to be negligible in the studied HM/Co systems.

We studied several magnetic bilayers (see Supplemental Material [19]), each of which underwent repeated cycles of measurements and annealing (see Table 1) to tune the strength of ISOC. These include sample series Pt 4/Co 0.85 (P1-P4) and $Au_{0.25}Pt_{0.75}$ 4/Co 0.85 (P5-P8) with perpendicular magnetic anisotropy (PMA), and Pt 4/Co 3.2 (I1-I4) with in-plane magnetic anisotropy (IMA) (the numbers are layer thicknesses in nm). In addition, we measured two IMA reference samples Pt 4/Hf 0.67/Co 1.4 (R1) and Pt 4/Co 1.4 (R2).

We used two quantities, the interfacial magnetic anisotropy energy density (K_s) and the anomalous Hall conductivity (σ_{AH}), as indicators of the strength of ISOC. It has been well established that K_s in HM/Co bilayers and superlattices originates from spin-orbit coupling (SOC)-enhanced orbital magnetic moments localized at the first layer adjacent to the interface [28,29]. A HM with a strong SOC (e.g. 5*d* Pt) can modify the perpendicular orbital moments in an adjacent 3*d* Co layer via strong interfacial 3*d*-5*d* hybridization, which enhances the latter's spin-orbit interaction and thereby K_s. σ_{AH} in thick Co films is determined by the intrinsic contribution from the internal spin-orbit interaction related to the integral of the Berry curvature over occupied states [30]. However, in ultrathin ferromagnetic films where the electron mean-free-path is determined by interfacial scattering, this "bulk" contribution to σ_{AH} decreases linearly towards zero with decreasing FM thickness, which allows the contribution from a strong

ISOC to dominate [31]. We find that σ_{AH} in ultrathin Co films in contact with Pt (or $Au_{0.25}Pt_{0.75}$) provides a separate and independent measure of the relative strength of ISOC. In Figs. 1(a) and 1(b) we plot K_s and σ_{AH} as measured [19] in the different samples and for different annealing treatments. We note that the dominant contributions to the magnitudes of K_s (1-3.5 erg/cm^2) and σ_{AH} and their variation with annealing come from the Pt/Co and $Au_{0.25}Pt_{0.75}$/Co interfaces and their ISOC variation, rather than the MgO interfaces or bulk contributions. The upper bound for the K_s contribution from the Co-MgO interface is only ~0.6 erg/cm^2, i.e. K_s(MgO) as indicated by dotted line in Fig. 1(a). This bound was determined from a Pt/Hf/Co/MgO sample (R1) and assumes the Hf/Co interface has a negligible contribution to K_s. Upon 300˚C annealing, K_s(MgO) from R1 changed from 0.56±0.05 to 0.66±0.10 erg/cm^2, which is a minimal variation compared to that of the Pt/Co/MgO samples (e.g. nearly doubling from I1 to I2 for a similar 300 C anneal; also see [19]). Similarly, an upper bound for the Co bulk contribution to σ_{AH} is estimated to be 0.30×10^4 Ω^{-1} m^{-1} and 1.12×10^4 Ω^{-1} m^{-1} for the 0.85 and 3.2 nm "bulk" Co layers respectively, as indicated by σ_{AH}(Co) in Fig. 1(b), by using the σ_{AH}(Co) = 0.49×10^4 Ω^{-1} m^{-1} as determined from R1 and the proportional dependence of the intrinsic σ_{AH} on FM thickness [31]. There was also only a minimal effect of annealing on σ_{AH} of R1 (σ_{AH} = 0.46×10^4 Ω^{-1} m^{-1} after 300˚C annealing).

As is clearly seen in Fig. 1, the changes in K_s and σ_{AH}, track each other fairly closely for each sample set, consistently indicating an evolution of ISOC with the annealing steps. Specifically, for the two PMA samples the ISOC first increases and then gradually drops back down, while for the IMA Pt/Co samples it goes up monotonically. We tentatively attribute the different behavior of the thicker IMA Co sample set to differences in strain relaxation that occur for different Co thicknesses, associated with the large lattice mismatch relative to Pt. We attribute the evolution of ISOC with the annealing steps to thermal tuning of the spin-orbit proximity effect [14,32]. It has been shown that a HM with strong SOC can modify the SOC in the interfacial region of an adjacent layer due to the spin-orbit proximity effect [14,32]. A particularly striking example is the enhanced SHE and quantum anomalous Hall effect in graphene [32,33]. The annealing-induced changes of K_s and σ_{AH} that we observe are unrelated to atomic inter-mixing at the HM/Co interfaces. Chemical depth profiling indicates displacement of the Co is at most at the single-atomic-layer level, while x-ray reflectivity indicates that annealing sharpens the HM/Co interfaces rather than inducing intermixing [19,34]. Detailed transport and magnetic characterization of the samples safely further exclude the occurrence of any substantial atomic inter-mixing in these samples. K_s and σ_{AH} are high in the as-grown state, and keep increasing with annealing for the IMA Pt/Co series (I1-I4), whereas an intermixed layer that is deliberately introduced (e.g. an alloy layer of $Co_{50}Pt_{50}$ or $Pt_3Co/Co_{50}Pt_{50}/Co_3Pt$) is found to substantially degrade K_s and σ_{AH} [19,35]. We note that our results are also consistent with the earlier finding that high-temperature annealing can separate Co out from initially chemically disordered CoPt alloys and therefore enhance the PMA of Pt/Co (111) superlattices [36].

In Figs. 1(c) and 1(d) we show the dampinglike and fieldlike SOT efficiencies for the samples before and after annealing as determined by harmonic response measurements [19,37,38]. Since the resistivities of both Pt and $Au_{0.25}Pt_{0.75}$ can change during the annealing process [19] and alter the SOT efficiencies per unit bias current density, $\xi^j_{DL(FL)}$, we show first the SOT efficiencies per *unit applied electric field*, $\xi^E_{DL(FL)} = \xi^j_{DL(FL)}/\rho_{HM}$ (ρ_{HM} is the HM resistivity), in Fig. 1(c), and then for completeness $\xi^j_{DL(FL)}$ in Fig. 1(d). The dependence on annealing is similar for both quantities, but in the following we will focus on $\xi^E_{DL(FL)}$ as being more fundamental for considering changes in intrinsic SOTs.

Focusing first on the technologically more important and stronger dampinglike component ξ^E_{DL} for the PMA series Pt/Co (P1-P4) and $Au_{0.25}Pt_{0.75}$/Co (P5-P9), upon the first annealing step ξ^E_{DL} drops by ~50% and then gradually recovers back to some extent as result of the two subsequent annealing steps. For the IMA Pt/Co series (I1-I4), ξ^E_{DL} monotonically *decreases* with annealing. The key observation is that for all three cases the variations of ξ^E_{DL} upon annealing are strikingly well (negatively) correlated with the variation of the ISOC strength as seen in both Figs. 1(a) and 1(b). The fact that ξ^E_{DL} tracks the ISOC quantified by K_s and σ_{AH} in a markedly close manner strongly indicates that SML is mainly due to interfacial spin-orbit scattering. Our findings are consistent with the theoretical calculations [16-18] that a strong ISOC at the HM/FM interface enhances interfacial spin scattering. As schematically shown in Fig. 2(a), ISOC leads to a sharp drop and discontinuity of the spin current density at HM/FM interfaces in a SOT experiment.

In order to quantitatively determine the scaling of ξ^E_{DL} with ISOC, in Figs. 2(b) and 2(c) we plot ξ^E_{DL} as a function of the two more direct indicators of ISOC strength, K_s^{ISOC} = K_s - K_s(MgO) and σ_{AH}^{ISOC} = σ_{AH} - σ_{AH}(Co), for the three sample series. Strikingly, ξ^E_{DL} scales roughly linearly with K_s^{ISOC} and σ_{AH}^{ISOC} for each sample series. We also note that the intercepts are apparently indicating the values of ξ^E_{DL} in absence of the ISOC. It is rather remarkable that the best linear fits as a function of K_s^{ISOC} (σ_{AH}^{ISOC}) for both the PMA and IMA Pt/Co sample series indicate a giant ξ^E_{DL} of $\approx 6\times10^5$ Ω^{-1} m^{-1} for an ideal Pt/Co interface with zero ISOC. We point out that this large value $\xi^E_{DL} \approx 6\times10^5$ Ω^{-1} m^{-1} is still a lower bound for the internal spin Hall conductivity (σ_{SH}) of Pt, because the spin backflow (SBF) is not taken into account. If we assume the same SBF correction of T_{int}^{SBF} ≈0.48 for the Pt/Co interface as determined by a recent Pt thickness dependent study [39], we obtain $\sigma_{SH} \approx 1.3\times10^6$ Ω^{-1} m^{-1} for Pt. For the $Au_{0.25}Pt_{0.75}$/Co interface, the best linear fits of ξ^E_{DL} *vs* K_s^{ISOC} (σ_{AH}^{ISOC}) yield $\xi^E_{DL} \approx 7.5\times10^5$ Ω^{-1} m^{-1} in the zero-ISOC limit. Taking into account $T_{int}^{SBF} \approx$ 0.63 for $Au_{0.25}Pt_{0.75}$/Co interface as reported recently [40], we then obtain an internal value of $\sigma_{SH} \approx 1.2\times10^6$ Ω^{-1} m^{-1} for $Au_{0.25}Pt_{0.75}$, comparable with that of Pt. Here we emphasize that the strong ξ^E_{DL} variations are unlikely to be

attributed to any annealing-induced change of either $G^{\uparrow\downarrow}$ or the spin Hall conductivity of the HM layers. First, calculations have indicated that $G^{\uparrow\downarrow}$ is insensitive to interfacial disorder and ISOC [14-16], although recent work has suggested [16] that SBF at HM/FM interface could be modified by the interfacial spin-orbit scattering. Second, σ_{SH} for Pt and $Au_{1-x}Pt_x$ is dominated by the intrinsic SHE determined by the topology of the band structure, which for simple fcc metals is only dependent on the long-range crystal structure and is hence robust against localized changes in structural disorder that might occur during annealing [41]. We can also report that the strong variations in ξ^E_{DL} are unrelated to atomic intermixing at the HM/Co interface. We found that inserting a 0.6 nm intermixed Co-Pt layer (i.e. Pt_3Co 0.2/$Co_{50}Pt_{50}$ 0.2/Co_3Pt 0.2) between the Pt and Co had no significant effect on ξ^E_{DL}[19].

Our results indicate that the development of highly efficient HM/FM spin-torque devices, e.g. magnetic memories, will generally be advanced by *minimizing* ISOC at the HM/FM interfaces. As an example, we show in Figs. 3(a) and 3(b) that, through atomic Hf layer passivation of the HM/FM interface, the ISOC at a Pt/Co interface can be significantly reduced (samples R1 and R2), which beneficially results in an significant improvement of ξ^E_{DL} (and hence T_{int}) and a considerable reduction (×4.6) in the ISOC enhancement of magnetic damping via SML [7-9,16] or/and two-magnon scattering [42].

Turning to the fieldlike torque, for all the samples ξ^E_{FL} is negative (opposite to the Oersted field generated by the bias current) and small in magnitude compared to ξ^E_{DL} (Fig. 1(c)). According to the SBF theory, the fieldlike torque generated by a SHE spin current impinging onto a HM/FM interface is expected to be quite weak in comparison to the dampinglike torque [14], scaling as $ImG^{\uparrow\downarrow} << ReG^{\uparrow\downarrow}$. While the magnitude of $|\xi^E_{FL}|$ relative to ξ^E_{DL} for the Pt/Co and $Au_{.025}Pt_{0.75}$/Co samples is somewhat higher than predicted by these model calculations it is still comparatively low, consistent with other Pt/Co systems [9]. We find that $|\xi^E_{FL}|$ shows the same trend as that of ξ^E_{DL} with annealing, which we take as strong evidence that the SHE is the dominant mechanism for both torque components in our PMA and IMA samples, with ISOC determining the SML at the HM/Co interface.

Recent theoretical work [14,15,17] has advanced the understanding that there are various mechanisms by which a strong ISOC might generate rather than degrade SOTs in HM/FM bilayers. However, we find no indication of any significant ISOC-induced SOTs that scale positively with ISOC strength. Therefore, we conclude that the SOTs in the HM/Co systems studied here are predominantly due to the SHE in the HMs while the ISOC-generated torques are negligible.

In summary, we have demonstrated that thermal engineering of the spin-orbit proximity effect is a simple but effective approach to controllably vary the strength of ISOC at Pt/Co and $Au_{25}Pt_{75}$/Co interfaces. From this variation, we have obtained conclusive experimental evidence that ISOC at a HM/FM interface is the dominant mechanism for SML and increasing ISOC significantly reduces the dampinglike and fieldlike SOTs by enhancing interfacial spin scattering and degrading T_{int} in a linear manner. For both PMA and IMA HM/FM systems studied here, the ISOC-generated torques are negligible. This work also indicates that the development of highly efficient HM/FM spin-torque devices, e.g. magnetic memories, will generally be advanced by *minimizing* ISOC effects, through atomic layer passivation of the HM/FM interface or other means. The approach we utilized here to tune the ISOC strength should be also beneficial for research and applications of Dzyaloshinskii-Moriya interaction (skyrmion and chiral domain wall physics) and other ISOC effects.

This work was supported in part by the Office of Naval Research and by the NSF MRSEC program (DMR-1719875) through the Cornell Center for Materials Research. Support was also provided by the Office of the Director of National Intelligence (ODNI), Intelligence Advanced Research Projects Activity (IARPA), via contract W911NF-14-C0089. The views and conclusions contained herein are those of the authors and should not be interpreted as necessarily representing the official policies or endorsements, either expressed or implied, of the ODNI, IARPA, or the U.S. Government. The U.S. Government is authorized to reproduce and distribute reprints for Governmental purposes notwithstanding any copyright annotation thereon. Additionally this work was supported by the NSF (ECCS-1542081) through use of the Cornell Nanofabrication Facility/National Nanofabrication Infrastructure Network.

[1] I. M. Miron *et al*., Perpendicular switching of a single ferromagnetic layer induced by in-plane current injection, Nature **476**, 189–193 (2011).
[2] C. O. Avci *et al*., Current-induced switching in a magnetic insulator, Nat. Mater. **16**, 309–314 (2017).
[3] S. Emori, U. Bauer, S.-M. Ahn, E. Martinez, and G.S.D. Beach, Current-driven dynamics of chiral ferromagnetic domain walls, Nat. Mater. **12**, 611–616 (2013).
[4] L. Liu *et al*., Spin-torque switching with the giant spin Hall effect of tantalum, Science, **336**, 555 (2012).
[5] P. P. J. Haazen *et al*., Domain wall depinning governed by the spin Hall effect, Nat. Mater. **12**, 299 (2013).
[6] S. Shi, Y. Ou, S.V. Aradhya, D. C. Ralph, and R. A. Buhrman, Fast, low-current spin-orbit torque switching of magnetic tunnel junctions through atomic modifications of the free layer interfaces, Phys. Rev. Applied **9**, 011002 (2018).
[7] Y. Liu, Z. Yuan, R. J. H. Wesselink, A. A. Starikov, P. J. Kelly, Interface enhancement of Gilbert damping from first principles, Phys. Rev. Lett. **113**, 207202 (2014).
[8] J.-C.N. Rojas-Sánchez *et al*. Spin pumping and inverse spin Hall effect in platinum: the essential role of spin-memory loss at metallic interfaces, Phys. Rev. Lett. **112**, 106602 (2014).
[9] C.-F. Pai, Y. Ou, L. H. Vilela-Leao, D. C. Ralph, and R. A. Buhrman, Dependence of the efficiency of spin Hall torque on the transparency of Pt/ferromagnetic layer interfaces, Phys. Rev. B **92**, 064426 (2015).
[10] M. Zwierzycki, Y. Tserkovnyak, P. J. Kelly, A. Brataas, and G.E.W. Bauer, First-principles study of magnetization relaxation enhancement and spin transfer in thin magnetic films, Phys. Rev. B **71**, 064420 (2005).

[11] W. Zhang, W. Han, X. Jiang, S.-H. Yang, and S. S. P. Parkin, Role of transparency of platinum-ferromagnet interface in determining intrinsic magnitude of spin Hall effect, Nat. Phys. **11**, 496–502 (2015).
[12] P. M. Haney, H.-W. Lee, K.-J. Lee, A. Manchon, and M. D. Stiles, Current induced torques and interfacial spin-orbit coupling: Semiclassical modeling, Phys. Rev. B **87**, 174411 (2013).
[13] Y. Tserkovnyak, A. Brataas, and G. E. W. Bauer, Enhanced Gilbert damping in thin ferromagnetic films, Phys. Rev. Lett. **88**, 117601 (2002).
[14] P. M. Haney, H. W. Lee, K. J. Lee, A. Manchon, and M. D. Stiles, Current-induced torques and interfacial spin-orbit coupling, Phys. Rev. B **88**, 214417 (2013).
[15] K.-W. Kim, K.-J. Lee, J. Sinova, H.-W. Lee, and M. D. Stiles, Spin-orbit torques from interfacial spin-orbit coupling for various interfaces, Phys. Rev. B **96**, 104438 (2017).
[16] K. Chen and S. Zhang, Spin pumping in the presence of spin-orbit coupling, Phys. Rev. Lett. **114**, 126602 (2015).
[17] J. Borge and I. V. Tokatly, Ballistic spin transport in the presence of interfaces with strong spin-orbit coupling, Phys. Rev. B **96**, 115445 (2017).
[18] K. Dolui and B. K. Nikolić, Spin-memory loss due to spin-orbit coupling at ferromagnet/heavy-metal interfaces: *Ab initio* spin-density matrix approach, Phys. Rev. B 96, 220403(R)(2017).
[19] see Supplemental Material for more details on sample fabrication and characterizations, interfacial magnetic anisotropy and anomalous Hall conductivity, annealing effects on Pt/Co and Pt/Hf/Co interfaces, spin-orbit torque efficiencies and resisitivities, absence of relation of ISOC variations and SOTs variations to intermixing at the HM/Co interfaces, direct structural characterizations of the HM/Co interfaces, and strain variation. Supplemental Material includes Refs. [20-26].
[20] M. Hayashi, J. Kim, M. Yamanouchi, and H. Ohno, Quantitative characterization of the spin-orbit torque using harmonic Hall voltage measurements, Phys. Rev. B 89, 144425 (2014).
[21] J. Torrejon *et al*. Interface control of the magnetic chirality in CoFeB/MgO heterostructures with heavy-metal underlayers, Nat. Commun. **5**, 4655 (2014).
[22] Y. Ou, S. Shi, D. C. Ralph, R. A. Buhrman, Origin of fieldlike spin-orbit torques in heavy metal/ferromagnet/ oxide thin film heterostructures, Phys. Rev. B 94, 140414(R) (2016).
[23] R. J. Elliott, Theory of the effect of spin-orbit coupling on magnetic resonance in some semiconductors, Phys. Rev. 96, 266 (1954).
[24] Y. Yafet, g factors and spin-lattice relaxation of conduction electrons, Solid State Phys. 14, 1 (1963).
[25] Y. Ou, D. C. Ralph, R. A. Buhrman, Strong Enhancement of the Spin Hall Effect by Spin Fluctuations near the Curie Point of Fe_xPt_{1-x} Alloys, Phys. Rev. Lett. 120, 097203(2018).
[26] K. Yakushiji *et al*. Ultrathin Co/Pt and Co/Pd superlattice films for MgO-based perpendicular magnetic tunnel junctions, Appl. Phys. Lett. **97**, 232508 (2010).
[27] P. C. McIntyre, D. T. Wu, and M. Nastasi, Interdiffusion in epitaxial Co/Pt multilayers, J. Appl. Phys. **81**, 637 (1997).
[28] N. Nakajima *et al*. Perpendicular magnetic anisotropy caused by interfacial hybridization via enhanced orbital moment in Co/Pt multilayers: magnetic circular x-ray dichroism study, Phys. Rev. Lett. **81**, 5229-5232 (1998).
[29] M. Suzuki *et al*. Depth profile of spin and orbital magnetic moments in a subnanometer Pt film on Co, Phys. Rev. B **72**, 054430 (2005).
[30] D. Hou, Y. Li, D. Wei, D. Tian, L. Wu, and X. Jin, The anomalous Hall effect in epitaxial face-centered-cubic cobalt films, J. Phys.: Condens. Matter. **24**, 482001 (2012).
[31] L. Wu, K. Zhu, D. Yue, Y. Tian, and X. Jin, Anomalous Hall effect in localization regime, *Phys. Rev. B* **93**, 214418 (2016).
[32] A. Avsar *et al*. Spin–orbit proximity effect in graphene, Nat. Commun. **5**, 4875 (2014).
[33] Z. Qiao *et al*. Quantum anomalous Hall Effect in graphene proximity coupled to an antiferromagnetic insulator, Phys. Rev. Lett. **112**, 116404 (2014).
[34] L. J. Zhu, D. C. Ralph, R. A. Buhrman, Irrelevance of magnetic proximity effect to spin-orbit torques in heavy metal/ferromagnet bilayers, Phys. Rev. B **98**,134406 (2018).
[35] P. Poulopoulos *et al*. Structural, magnetic, and spectroscopic magneto-optical properties aspects of Pt–Co multilayers with intentionally alloyed layers, J. Appl. Phys. **94**, 7662 (2003).
[36] W. Grange *et al*. Experimental and theoretical x-ray magnetic-circular-dichroism study of the magnetic properties of $Co_{50}Pt_{50}$ thin films, Phys. Rev. B 62, 1157 (2000).
[37] J. Kim, J. Sinha, M. Hayashi, M. Yamanouchi, S. Fukami, T. Suzuki, S. Mitani, and H. Ohno, Layer thickness dependence of the current-induced effective field vector in Ta|CoFeB|MgO, Nat. Mater. **12**, 240–245 (2013).
[38] C. O. Avci, K. Garello, M. Gabureac, A. Ghosh, A. Fuhrer, S. F. Alvarado, and P. Gambardella, Interplay of spin-orbit torque and thermoelectric effects in ferromagnet/normal-metal bilayers. Phys. Rev. B 90, 224427 (2014).
[39] M.-H. Nguyen, D. C. Ralph, and R. A. Buhrman, Spin torque study of the spin Hall conductivity and spin diffusion length, Phys. Rev. Lett. **116**, 126601 (2016).
[40] L. Zhu, D. C. Ralph, and R. A. Buhrman, Efficient spin current generation by the spin Hall effect in $Au_{1-x}Pt_x$, Phys. Rev. Applied 10, 031001 (2018).
[41] E. Vilanova Vidal, H. Schneider, and G. Jakob, Influence of disorder on anomalous Hall effect for Heusler compounds, Phys. Rev. B 83, 174410 (2011).
[42] R. Arias and D. L. Mills, Extrinsic contributions to the ferromagnetic resonance response of ultrathin films. Phys. Rev. B **60**, 7395-7408 (1999).

Table 1. Sample configurations and annealing conditions. Bilayers P1-P8 have perpendicular magnetic anisotropy, while others have in-plane magnetic anisotropy. Layer thicknesses for Co, Pt, $Au_{0.25}Pt_{0.75}$ and Hf are in nm.

#	Bilayers	Anneal condition
P1	Pt 4/Co 0.85	As-grown
P2	Pt 4/Co 0.85	350 °C,2 h
P3	Pt 4/Co 0.85	350 °C,4 h
P4	Pt 4/Co 0.85	350 °C,4 h +400 °C,1 h
P5	$Au_{0.25}Pt_{0.75}$ 4/Co 0.85	As-grown
P6	$Au_{0.25}Pt_{0.75}$ 4/Co 0.85	350 °C,2 h
P7	$Au_{0.25}Pt_{0.75}$ 4/Co 0.85	350 °C,4 h
P8	$Au_{0.25}Pt_{0.75}$ 4/Co 0.85	350 °C,4 h +400 °C,1 h
I1	Pt 4/Co 3.2	As-grown
I2	Pt 4/Co 3.2	300 °C, 0.5 h
I3	Pt 4/Co 3.2	300 °C, 0.5 h +350 °C,4 h
I4	Pt 4/Co 3.2	300 °C,0.5 h +350 °C,4 h+450 °C,1 h
R1	Pt 4/ Hf 0.67/ Co 1.4	As-grown/ 300 °C, 0.5 h
R2	Pt 4/ Co 1.4	As-grown

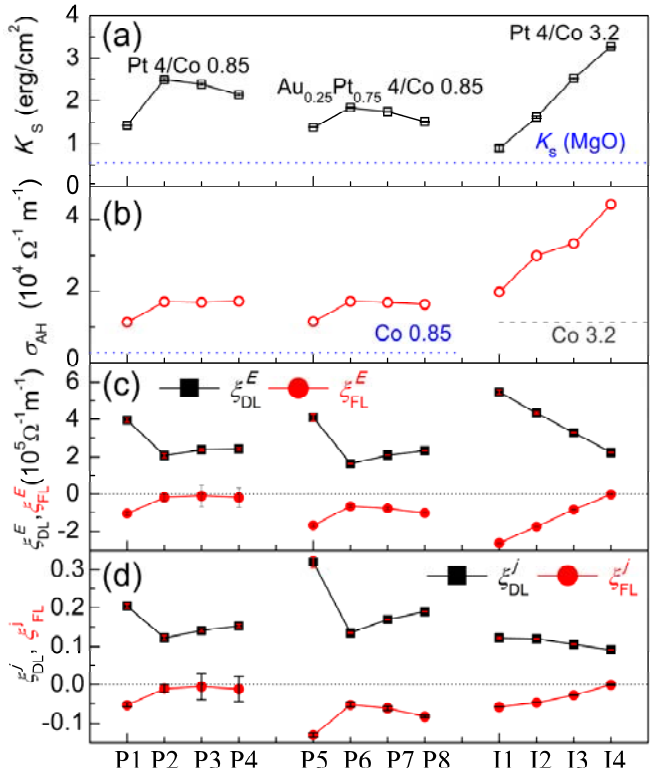

Fig. 1. (a) The interfacial magnetic anisotropy energy density (K_s), (b) The anomalous Hall conductivities (σ_{AH}), (c) The dampinglike and fieldlike SOT efficiencies per unit applied electric field, and (d) The dampinglike and fieldlike SOT efficiencies per unit bias current density for the sample series defined in Table 1. The blue dotted line in (a) represents an upper bound for K_s from the Co/MgO interface as determined from measurement of the R1 reference sample with Hf passivation of the interface; the blue dotted and grey dashed lines in (b) represent calculated values of σ_{AH} for a 0.85 nm Co layer and a 3.2 nm Co layer, respectively, in the absence of significant ISOC at the HM/Co interface.

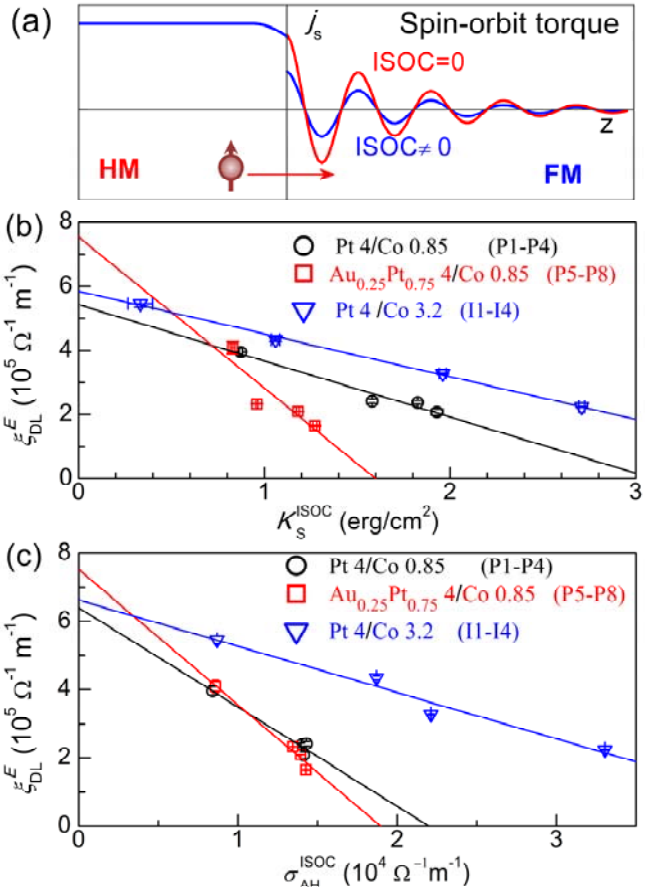

Fig. 2. (a) Schematic illustration of the z-profile of the spin current density (j_s) at a HM/FM interface in spin-orbit torque experiment, where the spin current arises from the SHE in the bulk of the HM. The blue and red curves represent j_s for non-zero and zero ISOC at the HM/FM interface, respectively. The red arrow points to the spin transport direction. In the case of non-zero ISOC, j_s drops when traveling across the interface. Scaling of dampinglike SOT efficiency per unit applied electric field with (b) the interfacial magnetic anisotropy energy density (K_s^{ISOC}) at the HM/Co interface, and (c) the HM/Co interface contribution to the anomalous Hall conductivity (σ_{AH}^{ISOC}), for the sample series defined in Table 1. The solid lines in (b) and (c) represent the best linear fits to the data.

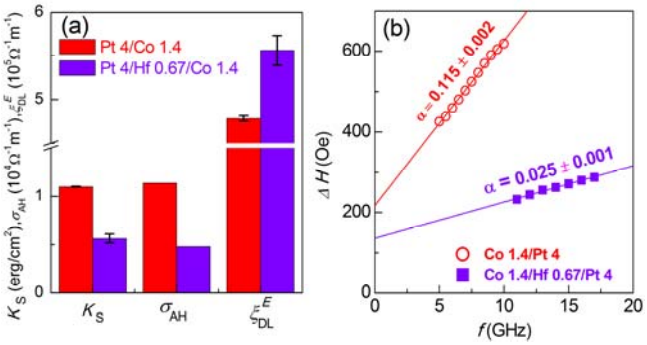

Fig. 3. (a) The interfacial magnetic anisotropy energy density (K_s), the anomalous Hall conductivities (σ_{AH}), and dampinglike SOT efficiency per unit applied electric field (ξ_{FL}^E), and (b) Frequency dependence of ferromagnetic resonance linewidth broadening (ΔH) and magnetic damping constant (α) for Pt 4/Co 1.4 and Pt 4/Hf 0.67/Co 1.4 as-grown samples.